CRYSTAL GROWTH & DESIGN

pubs.acs.org/crystal

Article

Solvent and Solvate Effects on the Cocrystallization of C_{60} with Co^{II}(OEP) or Zn^{II}(OEP) (OEP = Octaethylporphyrin)

Mrittika Roy, Isaac D. Diaz Morillo, Xian B. Carroll, Marilyn M. Olmstead,* and Alan L. Balch*

Cite This: *Cryst. Growth Des.* 2020, 20, 5596−5609

Read Online

ACCESS | Metrics & More | Article Recommendations | Supporting Information

ABSTRACT: Variations in crystallization conditions produce dramatic changes in the composition and geometry of solvated porphyrin-fullerene cocrystals. The products obtained by cocrystallization from a benzene solution of C_{60} with a solution of M^{II}(OEP) (M = Co or Zn) in a variety of solvents have been analyzed crystallographically. The cocrystals fall into three categories: Class 1, ordered crystals with a 1:1 porphyrin/fullerene ratio (Co^{II}(OEP)·C_{60}·CS_2 (**1**), Zn^{II}(OEP)·C_{60}·CS_2 (**2**), Co^{II}(OEP)·C_{60}·$C_4H_8O_2$ (**5**), Co^{II}(OEP)·C_{60}·1.5C_6H_6 (**8**); Class 2, ordered crystals with a 2:1 porphyrin/fullerene ratio (2Zn^{II}(OEP)·C_{60}·0.75CCl_4 (**4**) and 2Co^{II}(OEP)·C_{60}·C_4H_8O (**7**)); and Class 3, crystals involving a five-coordinate metal and a disordered fullerene cage ($ClCo^{III}$(OEP)·C_{60}·CCl_4 (**3**) and ($C_4H_8O_2$)Zn^{II}(OEP)·C_{60}·$C_4H_8O_2$ (**6**)). Class 1 crystals form in three different space groups, yet all contain two packing motifs: columns with significant porphyrin/porphyrin, fullerene/porphyrin, and fullerene/fullerene interactions and zigzag chains of fullerenes. Class 2 crystals are isostructural. Class 3 crystals vary due to differing axial ligands. Whether crystals with a 1:1 or 2:1 porphyrin/C_{60} ratio form depends upon the solvent rather than the amounts of components present in solution. Cocrystallization using Zn^{II}(OEP) and chlorinated solvents appears as the preferred combination to produce ordered C_{60} molecules, and this situation may pertain for other fullerenes.

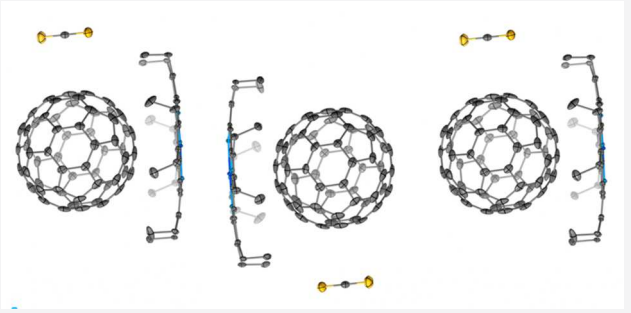

INTRODUCTION

The discovery of fullerenes,[1,2] closed carbon cages with clearly defined interior and exterior surfaces, produced an array of unusual soluble molecules with sizes that begin with C_{60} but can extend up to at least C_{418}.[3,4] Naturally, the structures of these molecules are a significant key to understanding their properties. Single-crystal X-ray diffraction is an ideal method to determine the structures of such molecules. However, the rather uniform surfaces of these molecules, which are constructed from pentagons and hexagons only, frequently allow for disorder within crystals. For example, crystalline C_{60} alone displayed twinning and orientational disorder even at 110 K.[5,6] Crystallization of fullerenes from a solution frequently produces solvated crystals. While many of these solvates also display disorder, in several cases structural information could be obtained by cooling the solvated crystal to 90 K.[7]

In 1999, reports of the cocrystallization of the fullerenes and endohedral metallofullerenes with metalloporphyrins appeared.[8−10] One result of these observations was the design and synthesis of a number of porphyrin-containing host molecules and metal−organic frameworks that could encapsulate various fullerenes and might be used for the separation of these carbon cages.[11−15] Additionally, Ni^{II}(OEP) has been successfully used as a cocrystallization agent for the structural characterization of newly prepared and isolated fullerenes and endohedral fullerenes. In such cocrystals, the eight beta-ethyl group arms typically embrace the fullerene cage. Thus, cocrystallization with Ni^{II}(OEP) has produced structural identification of three isomers of C_{90}[16,17] and two isomers of C_{96}.[18] Cocrystallization with Ni^{II}(OEP) has also been used to identify the structures of endohedral fullerenes such as $Sc_3N@I_h$-C_{80}, $Sc_4O_2@I_h$-C_{80},[19] $Sc_4O_3@I_h$-C_{80},[20] $Sm_2@D_{3d}$(822)-C_{104},[21] and $Y_2C_2@C_1$(1660)-C_{108}.[22] Such cocrystallizations have also allowed the identification of a number of endohedral fullerenes ($Sc_3N@D_3$(6140)-C_{68},[23] $Gd_3N@C_s$(39663)-C_{82},[24] $Sc_2@C_{2v}$(4059)-C_{66},[25] $LaSc_2N@C_s$(hept)-C_{80},[26] and $Sc_2C_2@C_s$(hept)-C_{88}[27]) that do not obey the isolated pentagon rule (IPR). The IPR, which is followed by all known pristine empty cage fullerenes, requires that each of the 12 pentagons in a fullerene be surrounded by five hexagons.

Although cocrystallization of fullerenes with Ni^{II}(OEP) has been used to determine the structures of endohedral fullerenes[28−31] and fullerenes with holes in their surface[32,33]

Received: June 9, 2020
Revised: July 10, 2020
Published: July 10, 2020

https://dx.doi.org/10.1021/acs.cgd.0c00793
Cryst. Growth Des. 2020, 20, 5596−5609

by many different research groups, there are several factors that are involved in crystal growth, including the role of the specific metal ion in the porphyrin and the solvents and other variables in the crystallization process. Recently, we demonstrated that cocrystallization of C_{60} with M^{II}(OEP) with M = Co, Ni, Cu, and Zn showed significant differences among the four different metalloporphyrins.[34] For example, cocrystallization of Co^{II}(OEP) and Zn^{II}(OEP) with C_{60} from a benzene/dichloromethane mixture produced the remarkable crystals $6Co^{II}(OEP)\cdot 5C_{60}\cdot 5CH_2Cl_2$ and $6Zn^{II}(OEP)\cdot 5C_{60}\cdot 5CH_2Cl_2$, henceforth designated as **6:5Co** and **6:5Zn** respectively, that contained one C_{60} molecule sandwiched between two porphyrin molecules in a clam shell arrangement, one C_{60} molecule adjacent to only one porphyrin molecule, and one C_{60} molecule that made no contact with any porphyrin as seen in Figure 1. Compounds **6:5Co** and **6:5Zn** differ in two important aspects. In **6:5Zn**, the back-to-back pairs of Zn^{II}(OEP) molecules come much closer together than was the case for the corresponding cobalt cocrystal so that the Zn−N distances between adjacent molecules were in the range of 2.57−2.59 Å. Additionally, in **6:5Zn**, one of the ethyl groups on one of the three Zn^{II}(OEP) molecules in the asymmetric unit was not directed toward the adjacent C_{60} molecule. Under similar conditions, cocrystallization with Ni^{II}(OEP) and Cu^{II}(OEP) produced two other, different cocrystals, $Ni^{II}(OEP)\cdot C_{60}\cdot 0.1CH_2Cl_2\cdot 1.9C_6H_6$ and $Cu^{II}(OEP)\cdot C_{60}\cdot CH_2Cl_2$, each with only one porphyrin engaging a C_{60} molecule. That study demonstrated clear differences between the similar planar M^{II}(OEP) molecules in cocrystal composition and structure.

Here we address a separate issue: the effect of solvent on cocrystal composition and structure. Notice that the dichloromethane molecules in the structure of **6:5Co**, shown in Figure 1, sit off to the side of the columns of fullerenes and Co^{II}(OEP) molecules without forming any unusual contacts with the molecules in the column. Additionally, these crystals were grown from a dichloromethane/benzene mixture, but only dichloromethane was found in the cocrystal. This fact is noteworthy since benzene is known to display both π-type face-to-face and C−H—$\pi(C_{60})$ interactions with C_{60} in solvated crystals.[7,34−36] Consequently, benzene might have been expected to be favored for incorporation into the cocrystals as it did in the formation of $Ni^{II}(OEP)\cdot C_{60}\cdot 0.1CH_2Cl_2\cdot 1.9C_6H_6$ and $Ni^{II}(OEP)\cdot C_{60}\cdot 2C_6H_6$.[34] Would different combinations of solvents produce the same set of cocrystal compositions with similar structures, or would new types of cocrystals form? Could other solvent molecules simply replace the dichloromethane molecules present in **6:5Co** and **6:5Zn** as reported for the formation of the analogous solvates $6Co^{II}(OEP)\cdot 5C_{60}\cdot 5C_2H_4Cl_2$ and $6Zn^{II}(OEP)\cdot 5C_{60}\cdot 5C_2H_4Cl_2$? Here, we report results from the cocrystallization of C_{60} with Co^{II}(OEP) or Zn^{II}(OEP), the only two complexes of OEP known to form 2:1 clamshell arrangements with C_{60}, using a variety of solvents to dissolve the porphyrin.

RESULTS AND DISCUSSION

Cocrystal Growth. Crystals were grown using the slow diffusion technique. In a 5 mm outside diameter, 8-in. long glass tube, a solution of C_{60} in benzene was carefully layered over an equimolar solution of M^{II}(OEP) (M = Co or Zn) in the appropriate solvent as discussed below. For each combination of M^{II}(OEP) and solvent, the order of layering was also reversed to check for any resulting change. Crystals generally began appearing after a day, but they were allowed to grow for 2−3 weeks to obtain suitably sized crystals. In each case where crystals grew, only one type of crystal was found as confirmed by spot-checking the unit cells of at least three different crystals. Efforts to change cocrystal composition by altering the ratios of M^{II}(OEP) to C_{60} were not fruitful.

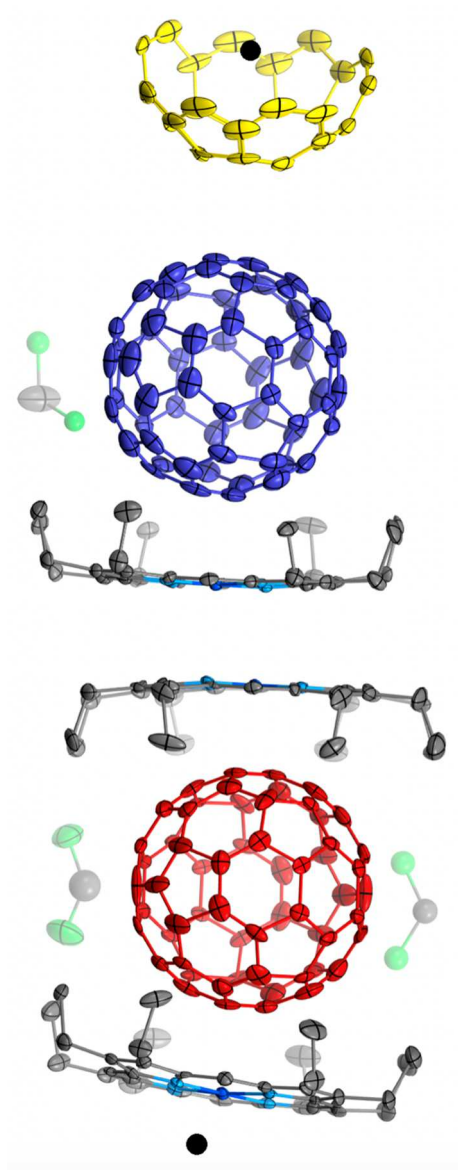

Figure 1. Columnar arrangement of fullerenes and Co^{II}(OEP) molecules in $6Co^{II}(OEP)\cdot 5C_{60}\cdot 5CH_2Cl_2$ or **6:5Co**. The asymmetric unit is shown with 50% thermal contours with black dots indicating the crystallographic centers of symmetry. The rest of the yellow-colored fullerene is generated by inversion through one of these centers. Hydrogen atoms and disorder in the dichloromethane molecules are omitted for clarity. Created from the data in Roy, M.; Olmstead, M. M.; Balch, A. L. *Cryst. Growth Des.* **2019**, *19*, 6743−6751.

*Comparison of the Structures of $Co^{II}(OEP)\cdot C_{60}\cdot CS_2$ (**1**) and $Zn^{II}(OEP)\cdot C_{60}\cdot CS_2$ (**2**).* Previous work has shown that crystals of **6:5Co** and **6:5Zn** formed when a solution of C_{60} in benzene was allowed to diffuse into a solution of Co^{II}(OEP) or Zn^{II}(OEP) in dichloromethane. However, when the metalloporphyrin was dissolved in carbon disulfide, the cocrystals, $Co^{II}(OEP)\cdot C_{60}\cdot CS_2$ (**1**) and $Zn^{II}(OEP)\cdot C_{60}\cdot CS_2$, formed.

https://dx.doi.org/10.1021/acs.cgd.0c00793
Cryst. Growth Des. 2020, 20, 5596−5609

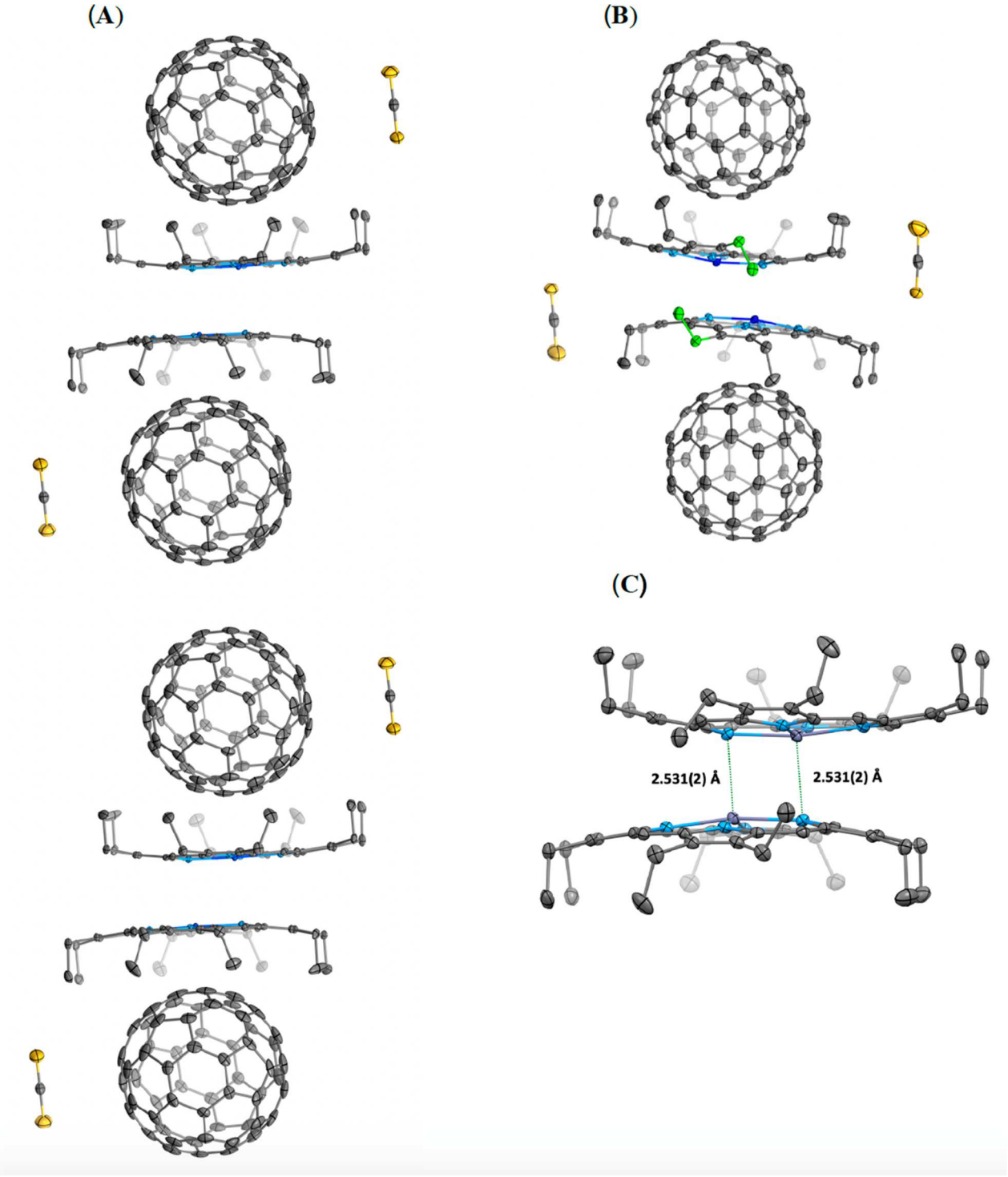

Figure 2. (A) The columnar structure of $P\bar{1}$ $Co^{II}(OEP)\cdot C_{60}\cdot CS_2$ (**1**). (B) A portion of the columnar structure of $I2/a$ $Zn^{II}(OEP)\cdot C_{60}\cdot CS_2$ (**2**). The ethyl arms of the $Zn^{II}(OEP)$ molecules that point away from the C60 molecule are colored green. (C) A diagram showing the short, out-of-plane Zn−N distance between two adjacent porphyrins in $Zn^{II}(OEP)\cdot C_{60}\cdot CS_2$ (**2**). Thermal contours are shown at the 50% level. Hydrogen atoms are omitted for clarity.

These crystals have a different stoichiometry and structure than **6:5Co** and **6:5Zn**, but they also have some properties in common with those cocrystals.

In $Co^{II}(OEP)\cdot C_{60}\cdot CS_2$ (**1**), which crystallizes in the space group $P\bar{1}$, the asymmetric unit consists of one molecule of each of the three components. Figure 2 shows the organization of C_{60} and $Co^{II}(OEP)$ molecules in $Co^{II}(OEP)\cdot C_{60}\cdot CS_2$ (**1**) into columns with the carbon disulfide molecules situated off to the sides of these columns. Along the column, two porphyrin molecules pack about a center of symmetry to produce a back-to-back array. Additionally, each porphyrin cups an adjacent C_{60} molecule. Finally, there is close contact between two C_{60} molecules, which pack about a center of symmetry with a centroid-to-centroid distance of 9.889 Å. This distance is the

https://dx.doi.org/10.1021/acs.cgd.0c00793
Cryst. Growth Des. 2020, 20, 5596−5609

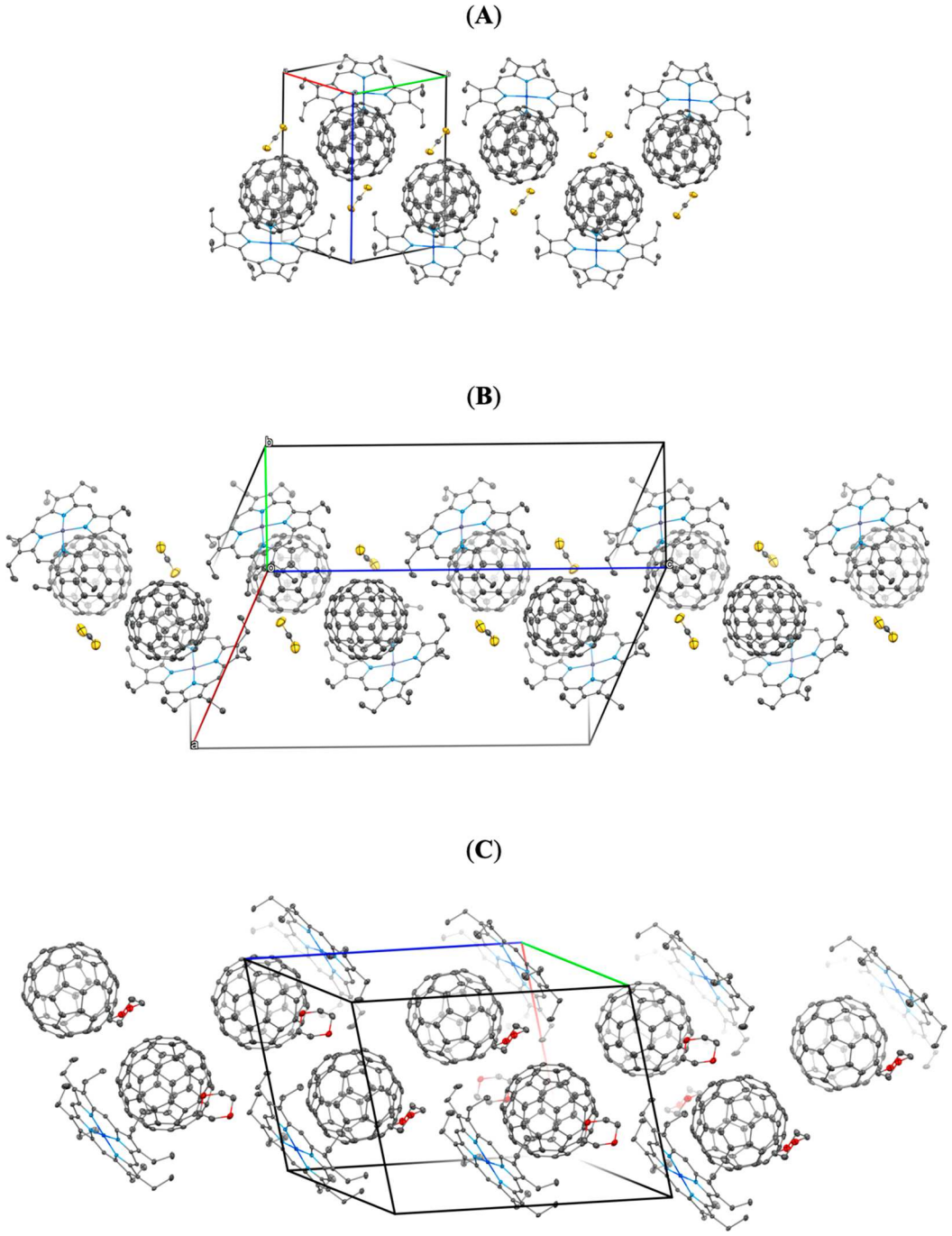

Figure 3. Molecular packing and unit cells in (A) $P\bar{1}$ $Co^{II}(OEP)\cdot C_{60}\cdot CS_2$ (**1**), (B) $I2/a$ $Zn^{II}(OEP)\cdot C_{60}\cdot CS_2$ (**2**), and (C) $P2_1/c$ $Co^{II}(OEP)\cdot C_{60}\cdot C_4H_8O_2$ (**5**) showing the zigzag similar arrangements of fullerenes in each. Hydrogen atoms are omitted for clarity.

shortest distance between two fullerene centroids in this crystal.

While $Zn^{II}(OEP)\cdot C_{60}\cdot CS_2$ (**2**) has the same composition as $Co^{II}(OEP)\cdot C_{60}\cdot CS_2$ (**1**), it crystallizes in a different space group, $I2/a$, with one molecule of each of the three components in the asymmetric unit. Nevertheless, columns similar to the one shown in Figure 2 are formed in this crystal. Figures SI-1 and SI-2 show how these columns relate to the unit cell for each cocrystal. Figure 2B shows a portion of that column, the portion that involves the back-to-back porphyrin/porphyrin interaction. In $Zn^{II}(OEP)\cdot C_{60}\cdot CS_2$ (**2**), this back-to-back arrangement arises from 2-fold crystallographic rotational symmetry.

In contrast to the situation in $Co^{II}(OEP)\cdot C_{60}\cdot CS_2$ (**1**) where all eight ethyl groups embrace the adjacent fullerene, in $Zn^{II}(OEP)\cdot C_{60}\cdot CS_2$ (**2**) only seven of the ethyl arms surround the neighboring C_{60} molecule. The unique ethyl group is colored green in Figure 2B and faces the reader. It is interesting to note that one ethyl arm in one of the three porphyrins in **6:5Zn** is also turned away from embracing the adjacent fullerene, while in the cobalt analogue, **6:5Co**, all ethyl arms in all three porphyrins in the asymmetric unit embrace the adjacent C_{60} molecule.[34]

Within the pair of adjacent porphyrins in $Zn^{II}(OEP)\cdot C_{60}\cdot CS_2$ (**2**), the molecules pack closely so that the interplanar Zn−N distance of 2.531(2) Å, as shown in Figure 2C, is rather

https://dx.doi.org/10.1021/acs.cgd.0c00793
Cryst. Growth Des. 2020, 20, 5596−5609

short, but still longer than an actual Zn−N axial bond distance, such as the Zn−N(pyridine) distance, 2.200(3) Å, in (pyridine)Zn^{II}(OEP).[37] In contrast, in Co^{II}(OEP)·C_{60}·CS_2, there is also a back-to-back interaction between two Co^{II}(OEP) molecules, but the Co−N distance, 2.883(2) Å is significantly longer than the comparable Zn−N distance in Zn^{II}(OEP)·C_{60}·CS_2 (**2**). This pattern of a close Zn−N distance but a longer Co−N distance between adjacent porphyrins is also present in the previously reported related pairs **6:5Zn** and **6:5Co**.

The molecular packing in Co^{II}(OEP)·C_{60}·CS_2 (**1**) in $P\bar{1}$ and Zn^{II}(OEP)·C_{60}·CS_2 (**2**) in *I*2/*a* shares other similarities beyond the columnar organization seen in Figures 2, SI-1, and SI-2. The structure of Co(OEP)·C_{60}·CS_2 (**1**) reveals a pattern of infinite zigzag chains with alternating centroid-to-centroid distances of the C_{60} molecules of 10.029 and 10.297 Å as seen in Figure 3A. Molecules of carbon disulfide occupy the cavities produced by the angular arrangement. These interactions are also supported by the "cups" of the Co(OEP) molecules. Another row of chains, perpendicular to this one and seen in Figure 2, is stacked by inversion and translation along *c*. This generates a third shorter centroid-to-centroid distance of 9.889 Å. For Zn^{II}(OEP)·C_{60}·CS_2 (**2**), similar zigzag arrangements of C_{60} molecules with carbon disulfide molecules in the adjoining spaces can be seen in Figure 3B. In this chain, the centroid-to-centroid distances between the C_{60} molecules are all the same, 10.101 Å.

*Comparison of the Structures of $ClCo^{III}$(OEP)·C_{60}·CCl_4 (**3**) and $2Zn^{II}$(OEP)·C_{60}·0.75CCl_4 (**4**).* With carbon tetrachloride as the solvent for Co^{II}(OEP), crystals of $ClCo^{III}$(OEP)·C_{60}·CCl_4 (**3**) formed. In this case, the cobalt complex was oxidized in a process that does not seem to have precedent but may involve adventitious dioxygen as the oxidant. The structure and relative orientations of the molecules within the cocrystal are shown in Figure 4 with the disorder removed. The disorder is shown in Figure SI-4. The $ClCo^{III}$(OEP) molecule utilizes all eight ethyl groups to embrace the fullerene, while the cobalt ion is drawn away from the fullerene toward the axial chloride ion. While the porphyrin is ordered, there is crystallographic disorder in the fullerene and the carbon tetrachloride molecule since they reside on sites with symmetry *m*2*m* in the space group *Cmcm*. Figure 5 shows the molecular packing for $ClCo^{III}$(OEP)·C_{60}·CCl_4 (**3**). Because of the presence of the axial chloride ligand, there is no back-to-back arrangement of the porphyrins. However, a zigzag pattern of C_{60} molecules is clearly present and similar to the zigzag arrays of fullerenes seen in Figure 5 for Co^{II}(OEP)·C_{60}·CS_2 (**1**) and Zn^{II}(OEP)·C_{60}·CS_2 (**2**)

When a benzene solution of C_{60} was allowed to diffuse into a solution of Zn^{II}(OEP) in carbon tetrachloride, $2Zn^{II}$(OEP)·C_{60}·0.75CCl_4(**4**) formed. In this case, two crystallographically independent Zn^{II}(OEP) molecules surrounded each fully ordered fullerene in a clamshell arrangement as seen in Figure 4B. Once again, all eight ethyl groups of each porphyrin surround the adjacent C_{60} molecule. The carbon tetrachloride molecule has only 0.75 fractional occupancy.

In $2Zn^{II}$(OEP)·C_{60}·0.75CCl_4 (**4**), the $2Zn^{II}$(OEP)·C_{60} units are organized into columns in which there is back-to-back contact between two porphyrins as seen in Figure 6. However, the Zn−N distance (2.609(3) Å) between adjoining porphyrins is much longer than the corresponding distance (2.531(2) Å) in Zn^{II}(OEP)·C_{60}·CS_2 (**2**) as seen in Figure 2. The carbon tetrachloride molecules are situated to the sides of these columns. The cell parameters and structure of

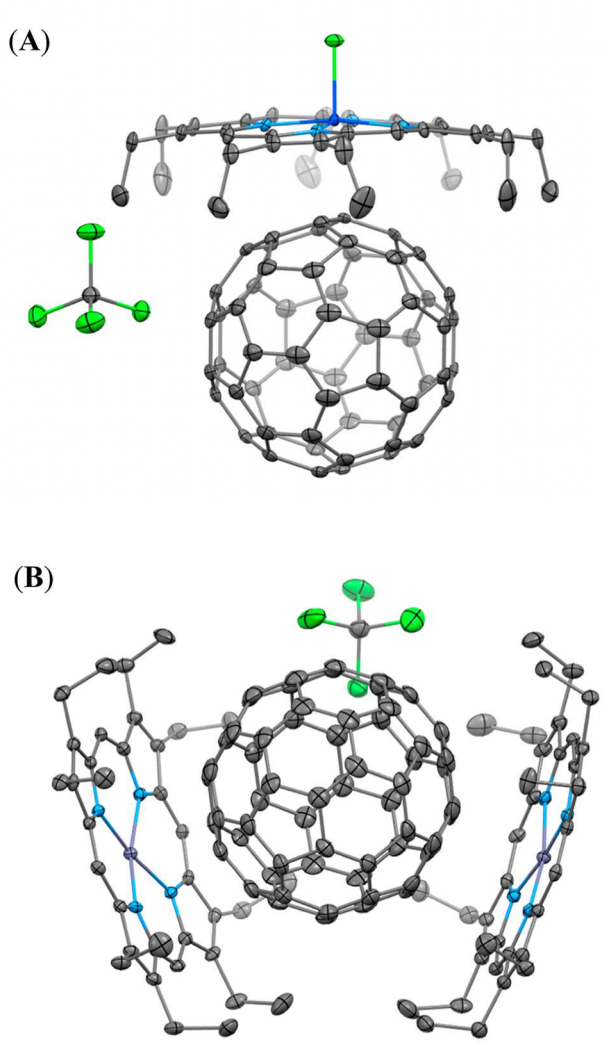

Figure 4. (A) The structure of $ClCo^{III}$(OEP)·C_{60}·CCl_4 (**3**). The disorder in the positions of the C_{60} and carbon tetrachloride molecules is not shown for simplicity. (B) The structure of $2Zn^{II}$(OEP)·C_{60}·0.75CCl_4 (**4**). Thermal contours are shown at the 50% level. Hydrogen atoms are omitted for clarity.

$2Zn^{II}$(OEP)·C_{60}·0.75CCl_4 (**4**) are similar to those of the previously reported $2Co^{II}$(OEP)·C_{60}·$CHCl_3$,[34] which has an analogous clamshell arrangement with two porphyrins surrounding each C_{60} molecule.

*Comparisons of the Dioxane Solvates, Co^{II}(OEP)·C_{60}·$C_4H_8O_2$ (**5**) and ($C_4H_8O_2$)Zn^{II}(OEP)·C_{60}·$C_4H_8O_2$ (**6**).* The dioxane solvates, Co^{II}(OEP)·C_{60}·$C_4H_8O_2$ (**5**) and ($C_4H_8O_2$)-Zn^{II}(OEP)·C_{60}·$C_4H_8O_2$ (**6**), are produced when dioxane is used as the solvent for the porphyrin. The structure of Co^{II}(OEP)·C_{60}·$C_4H_8O_2$ (**5**), which crystallizes in the space group $P2_1/c$ and contains one cobalt porphyrin, one fullerene, and one dioxane molecule in the asymmetric unit, is shown in (A) of Figure 7. The structure of Co^{II}(OEP)·C_{60}·$C_4H_8O_2$ (**5**) bears considerable similarity to that of Co^{II}(OEP)·C_{60}·CS_2 (**1**) and Zn^{II}(OEP)·C_{60}·CS_2 (**2**) shown in Figure 2, although each cocrystal belongs to a different space group. The fullerene is fully ordered with the eight ethyl groups of the porphyrin surrounding it. Co^{II}(OEP)·C_{60}·$C_4H_8O_2$ (**5**) packs into a column analogous to the one seen in Figure 2 for Co^{II}(OEP)·C_{60}·CS_2 (**1**). Figure 10 shows the face-to-face

https://dx.doi.org/10.1021/acs.cgd.0c00793
Cryst. Growth Des. 2020, 20, 5596−5609

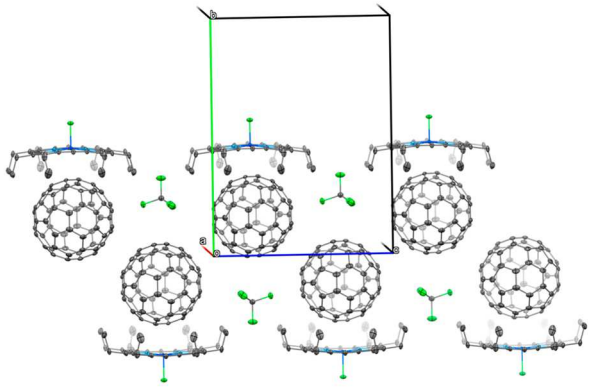

Figure 5. Molecular packing for $ClCo^{III}(OEP)\cdot C_{60}\cdot CCl_4$ (**3**) showing the zigzag arrangements of the fullerene molecules. The disorder in the positions of the C_{60} and carbon tetrachloride molecules is not shown for simplicity. Thermal contours are shown at the 50% level with hydrogen atoms omitted for clarity. To see this structure from a different perspective, see Figure SI-7.

interactions between two $Co^{II}(OEP)$ molecules and the positioning of the neighboring fullerenes in a portion of the column with the dioxane molecules situated beside the fullerenes. Figure SI-3 shows how these columns are arranged within the entire structure. The structure of $Co^{II}(OEP)\cdot C_{60}\cdot C_4H_8O_2$ (**5**) also involves a zigzag arrangement of fullerenes as shown in Figure 3C.

The structure of $(C_4H_8O_2)Zn^{II}(OEP)\cdot C_{60}\cdot C_4H_8O_2$ (**6**) shown in Figure 7B. This structure involves a fullerene that is disordered over two positions, an ordered $Zn^{II}(OEP)$ molecule that is coordinated by a disordered dioxane molecule, which occupies two sites, and an ordered dioxane molecule as a solvate. Figure 7 shows the major orientations of the fullerene and axial dioxane molecule, while Figure SI-5 shows the disorder. The zinc ion is located away from the fullerene, since it is coordinated to the axial dioxane ligand. The Zn−O distance is 2.277(3) Å. All eight ethyl groups surround the C_{60} molecule.

The molecular packing for $(C_4H_8O_2)Zn^{II}(OEP)\cdot C_{60}\cdot C_4H_8O_2$ (**6**) is shown in Figure 8. Zigzag arrangements of fullerene molecules are apparent and similar to those found in $ClCo^{III}(OEP)\cdot C_{60}\cdot CCl_4$ (**3**) as seen in Figure 5.

*The Tetrahydrofuran Solvate, $2Co^{II}(OEP)\cdot C_{60}\cdot C_4H_8O$ (**7**).* When a solution of C_{60} in benzene was allowed to diffuse into a solution of $Co^{II}(OEP)$ in tetrahydrofuran, the tetrahydrofuran-containing solvate, $2Co^{II}(OEP)\cdot C_{60}\cdot C_4H_8O$ (**7**) formed. A view of the asymmetric unit, which contains a molecule of each of the components, is shown in Figure 9. The clamshell structure of $2Co^{II}(OEP)\cdot C_{60}\cdot C_4H_8O$ (**7**) is similar to those of $2Zn^{II}(OEP)\cdot C_{60}\cdot 0.75CCl_4$ (**4**) described above and $2Co^{II}(OEP)\cdot C_{60}\cdot CHCl_3$,[34] but with different solvate molecules present in each crystal. All three of these cocrystals are found in the same space group, $P2_12_12_1$. Thus, the molecular packing for $2Co^{II}(OEP)\cdot C_{60}\cdot C_4H_8O$ (**7**) is similar to that shown in Figure 6 for $2Zn^{II}(OEP)\cdot C_{60}\cdot 0.75CCl_4$(**4**). Under similar crystallization conditions using $Zn^{II}(OEP)$, only low-quality crystals of what appeared to be a tetrahydrofuran solvate of C_{60} formed.

*The Benzene Solvate, $Co^{II}(OEP)\cdot C_{60}\cdot 1.5C_6H_6$ (**8**).* When benzene is the sole solvent for both the porphyrin and the fullerene, the new cocrystal, $Co^{II}(OEP)\cdot C_{60}\cdot 1.5C_6H_6$ (**8**), forms with cobalt and the known cocrystal, $2Zn^{II}(OEP)\cdot C_{60}\cdot C_6H_6$, is produced with zinc.[8] The asymmetric unit of $Co^{II}(OEP)\cdot C_{60}\cdot 1.5C_6H_6$ (**8**) consists of a single molecule of $Co^{II}(OEP)$, C_{60}, and benzene along with a half molecule of benzene with the other half generated by inversion through a center of symmetry. A portion of the columnar structure of $Co^{II}(OEP)\cdot C_{60}\cdot 1.5C_6H_6$ (**8**), which crystallizes in the space group $P\bar{1}$, is shown in Figure 10. The overall structure of $Co^{II}(OEP)\cdot C_{60}\cdot 1.5C_6H_6$ (**8**) is quite similar to that of

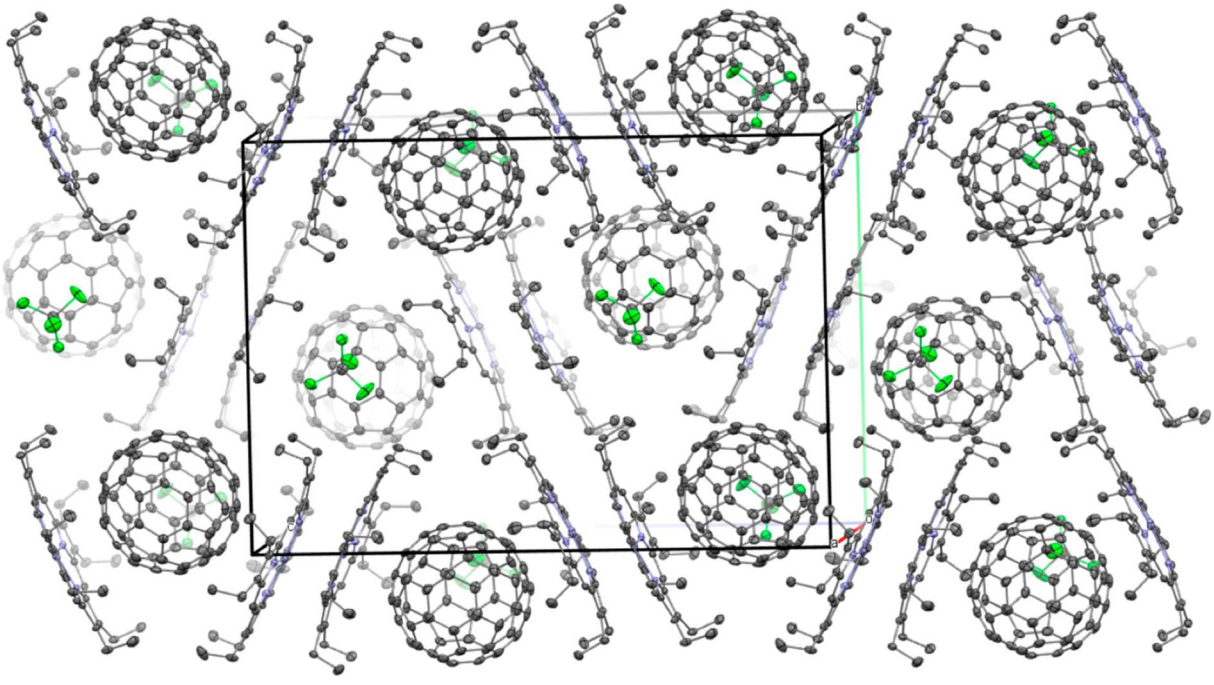

Figure 6. Molecular packing and unit cell for $2Zn^{II}(OEP)\cdot C_{60}\cdot 0.75CCl_4$ (**4**). Hydrogen atoms are omitted for clarity.

https://dx.doi.org/10.1021/acs.cgd.0c00793
Cryst. Growth Des. 2020, 20, 5596−5609

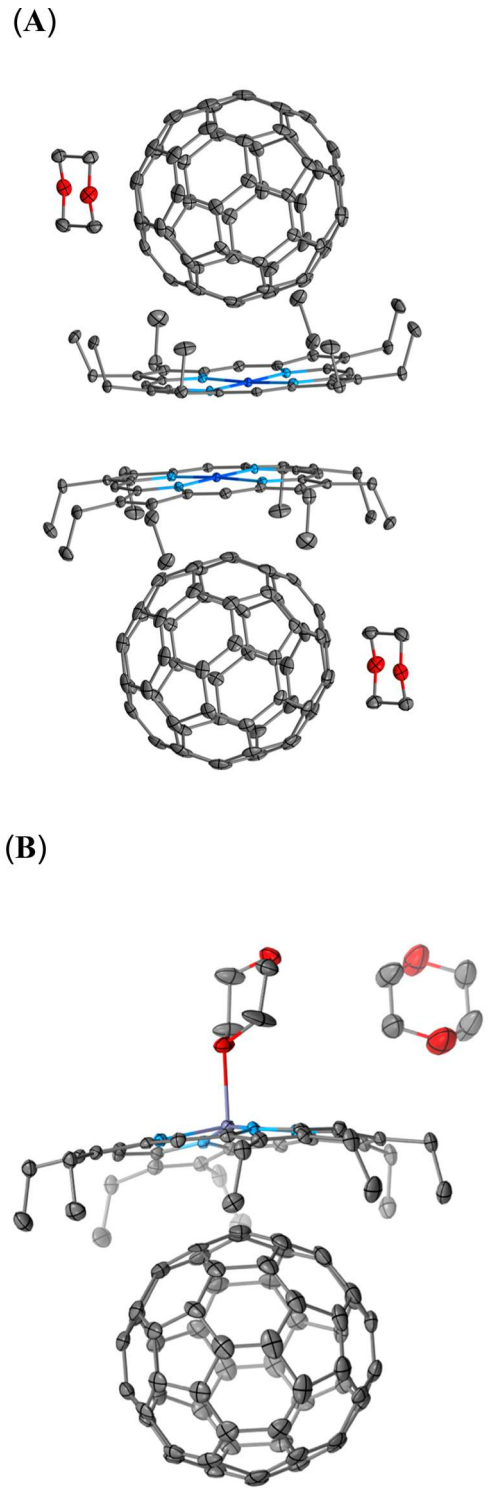

Figure 7. (A) A portion of the columnar structure of $Co^{II}(OEP)\cdot C_{60}\cdot C_4H_8O_2$ (**5**), which crystallizes in the space group $P2_1/c$, showing the back-to-back arrangements of the porphyrins and the locations of the solvate molecules beside the fullerene. (B) The structure of $(C_4H_8O_2)Zn^{II}(OEP)\cdot C_{60}\cdot C_4H_8O_2$ (**6**). Only the major positions of the C_{60} molecule (0.52684 fractional occupancy) and the coordinated dioxane (refined and displayed at 0.50 fractional occupancy) are shown. Thermal contours are shown at the 50% level, and hydrogen atoms are omitted for clarity.

$Co^{II}(OEP)\cdot C_{60}\cdot CS_2$ (**1**), which also forms in the space group $P\bar{1}$ Thus, both share the columnar structure shown in Figure 2 and the zigzag arrangement shown in Figure 3A. Crystals of $Co^{II}(OEP)\cdot C_{60}\cdot 1.5C_6H_6$ (**8**) are isostructural with the chlorobenzene solvate $Co^{II}(OEP)\cdot C_{60}\cdot 1.5C_6H_4Cl$, and the toluene solvate $Zn^{II}(OEP)\cdot C_{60}\cdot 1.5C_6H_5CH_3$.[38]

In contrast, the benzene solvate $2Zn^{II}(OEP)\cdot C_{60}\cdot C_6H_6$, has the clamshell structure found for $2Co^{II}(OEP)\cdot C_{60}\cdot C_4H_8O$ (**7**) and $2Zn^{II}(OEP)\cdot C_{60}\cdot 0.75CCl_4$ (**4**). These three cocrystals form in the same space group, $P2_12_12_1$.

Comparisons of Metalloporphyrin Structures. The porphyrin macrocycles in these cocrystals show some deviations from planarity as is common with such cocrystals. The various types of porphyrin distortions have been classified as ruffed, saddled, domed, waved (wav-(x) or wav-(y)), or pyrrole propellered.[39] Figure 11 shows diagrams representing the out-of-plane displacements of the porphyrin core atoms from the mean plane of the porphyrin for $Co^{II}(OEP)\cdot C_{60}\cdot CS_2$ (**1**), $Zn^{II}(OEP)\cdot C_{60}\cdot CS_2$ (**2**), $ClCo^{III}(OEP)\cdot C_{60}\cdot CCl_4$ (**3**), $2Zn^{II}(OEP)\cdot C_{60}\cdot 0.75CCl_4$ (**4**), $Co^{II}(OEP)\cdot C_{60}\cdot C_4H_8O_2$ (**5**), $(C_4H_8O_2)Zn^{II}(OEP)\cdot C_{60}\cdot C_4H_8O_2$ (**6**), $2Co^{II}(OEP)\cdot C_{60}\cdot C_4H_8O$ (**7**), $Co^{II}(OEP)\cdot C_{60}\cdot 1.5C_6H_6$ (**8**), $Co^{II}(OEP)$ alone,[40] and $Zn^{II}(OEP)$ alone.[41] The *y*-axis represents deviation or departure from planarity, which is calculated in each case by setting the plane to be the average of the four nitrogen and 20 sp^2 hybridized carbon atoms constructing the aromatic system, and then mapping the positive or negative deviation of each individual atom from the plane average. The *x*-axis represents a "linearized" form of a porphyrin macrocycle. In general, most of the porphyrins in this series show a dome distortion. The exception is five-coordinate $ClCo^{III}(OEP)\cdot C_{60}\cdot CCl_4$ (**3**), which has a wav-(y) distortion. This is in contrast to $(C_4H_8O_2)Zn^{II}(OEP)\cdot C_{60}\cdot C_4H_8O_2$(**6**) in (g), where the steric bulk and disorder in the axial ligand affects the four pyrroles unequally and causes the porphyrin to be severely domed. Notice that there is one pyrrole ring in (b) $Zn^{II}(OEP)\cdot C_{60}\cdot CS_2$ (**2**), (d) $2Zn^{II}(OEP)\cdot C_{60}\cdot 0.75CCl_4$ (**4**), and $2Zn^{II}(OEP)\cdot C_{60}\cdot 0.75CCl_4$ (**4**) that shows an unusually large out-of-plane distortion. These are the pyrrole rings that are involved with the close N−Zn contacts to the adjacent $Zn^{II}(OEP)$ molecule.

Table 1 presents information regarding the distances between the back-to-back porphyrin pairs for the cocrystals involving four-coordinate $M^{II}(OEP)$ and for $M^{II}(OEP)$ alone. The interplanar distance is calculated by first assigning "planes" as the average of 20 carbon and four nitrogen atoms constituting the aromatic system, and then averaging the perpendicular distance from each porphyrin plane to the centroid of its adjacent porphyrin plane. The lateral shift is the separation between the metal ions when one is projected onto the plane of the adjacent porphyrin, (see Figure SI-6 For details). Notice that the metal−metal distances, the interplanar distances, and the lateral shifts are all shorter in the cocrystals than they are in the pristine porphyrins, which crystallize with the metal on a crystallographic center of symmetry and four of the ethyl groups on one side of the porphyrin plane and four on the opposite side. The short interplanar distances and lateral shifts indicate that all of the porphyrin/fullerene cocrystals in Table 1 fall into the class of adjacent porphyrins with strong $\pi-\pi$ interactions according to the analysis proposed by Scheidt and Lee.[42] On the other hand, the pristine compounds $Co^{II}(OEP)$ and $Zn^{II}(OEP)$, with their long lateral shifts, fall into the class of adjacent porphyrins with weak $\pi-\pi$ interactions. Thus, there is a link between the

https://dx.doi.org/10.1021/acs.cgd.0c00793
Cryst. Growth Des. 2020, 20, 5596−5609

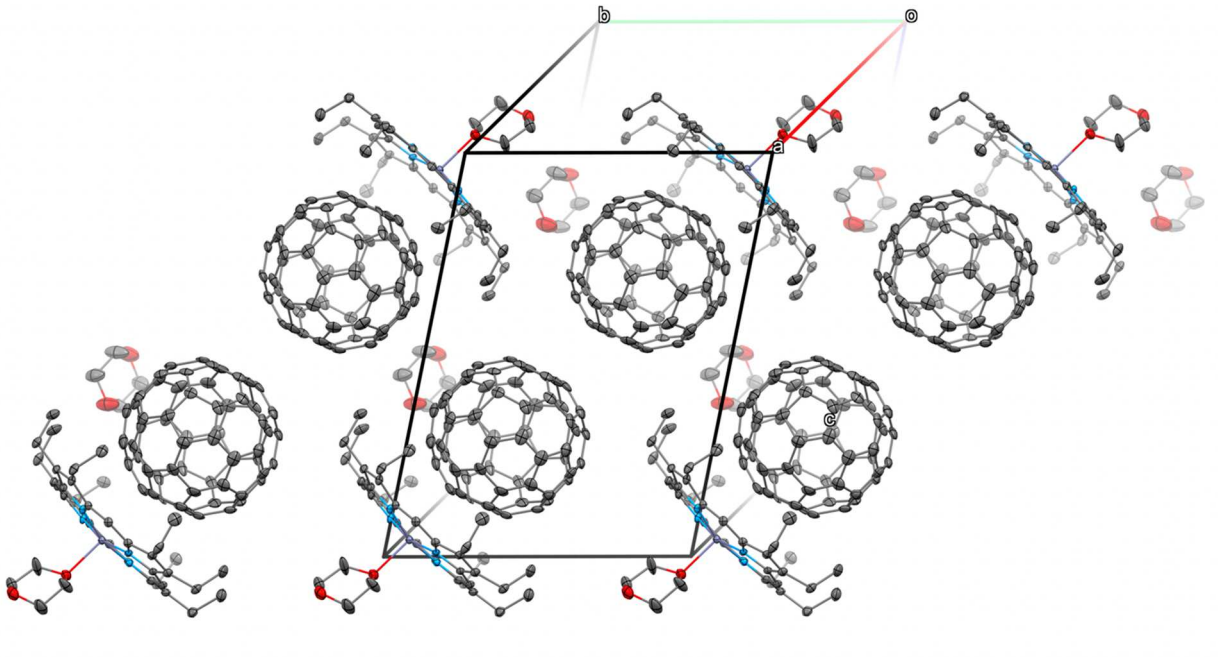

Figure 8. Molecular packing for $(C_4H_8O_2)Zn^{II}(OEP)\cdot C_{60}\cdot C_4H_8O_2$ (**6**) showing the zigzag arrangements of the fullerene molecules. The disorder in the positions of the C_{60} and axially coordinated dioxane molecules is not shown for simplicity. Thermal contours are shown at the 50% level with hydrogen atoms omitted for clarity. To see this structure from a different perspective, see Figure SI-8.

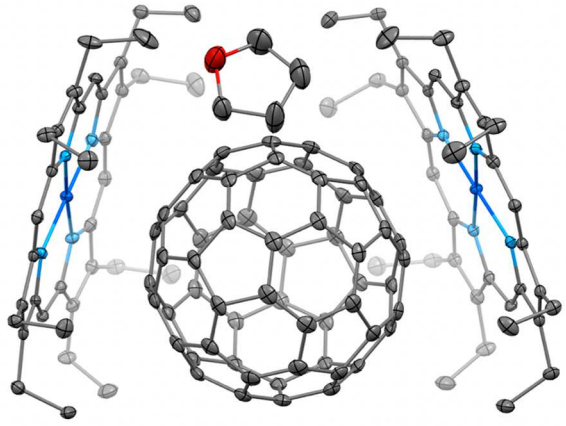

Figure 9. Structure of $2Co^{II}(OEP)\cdot C_{60}\cdot C_4H_8O$ (**7**). Thermal contours are shown at the 50% level. Hydrogen atoms are omitted for clarity.

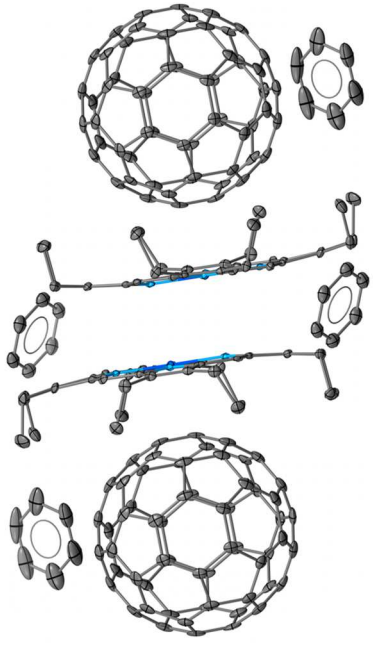

Figure 10. A section of the columnar structure of $Co^{II}(OEP)\cdot C_{60}\cdot 1.5C_6H_6$ (**8**). Thermal contours are shown at the 50% level, and hydrogen atoms are omitted for clarity.

fullerene/porphyrin and porphyrin/porphyrin interactions. Engaging a fullerene by a porphyrin using seven or eight ethyl arms to surround the fullerene promotes $\pi-\pi$ interaction with another porphyrin. The data in Table 1 also indicate that the closest out-of-plane M—N distances within pairs of porphyrins, the largest lateral shifts, and the closest metal—metal distances involve the zinc-containing cocrystals $Zn^{II}(OEP)\cdot C_{60}\cdot CS_2$ (**2**) and $2Zn^{II}(OEP)\cdot C_{60}\cdot 0.75CCl_4$ (**4**).

Nature of the $C_{60}/M^{II}(OEP)$ Interaction. In all the new structures reported here, the fullerene approached the metalloporphyrin so that two carbon atoms of a 6:6 ring junction are closest to the metal center. Relevant data are collected in Table 2. It is interesting that it is not the flat surfaces of a hexagon or a pentagon on the fullerene that make the closest contact to the porphyrin plane. Rather, a 6:6 ring junction with its olefinic character is positioned nearest to the metal in the porphyrin in all of these cocrystals.

The Solvent Dependence of Cocrystal Formation with $M^{II}(OEP)$. Table 3 presents a survey of the types of cocrystals found for $Co^{II}(OEP)$ and $Zn^{II}(OEP)$ using eight different solvents to dissolve the porphyrin with the fullerene in benzene solution. Different colors are used to identify

https://dx.doi.org/10.1021/acs.cgd.0c00793
Cryst. Growth Des. 2020, 20, 5596−5609

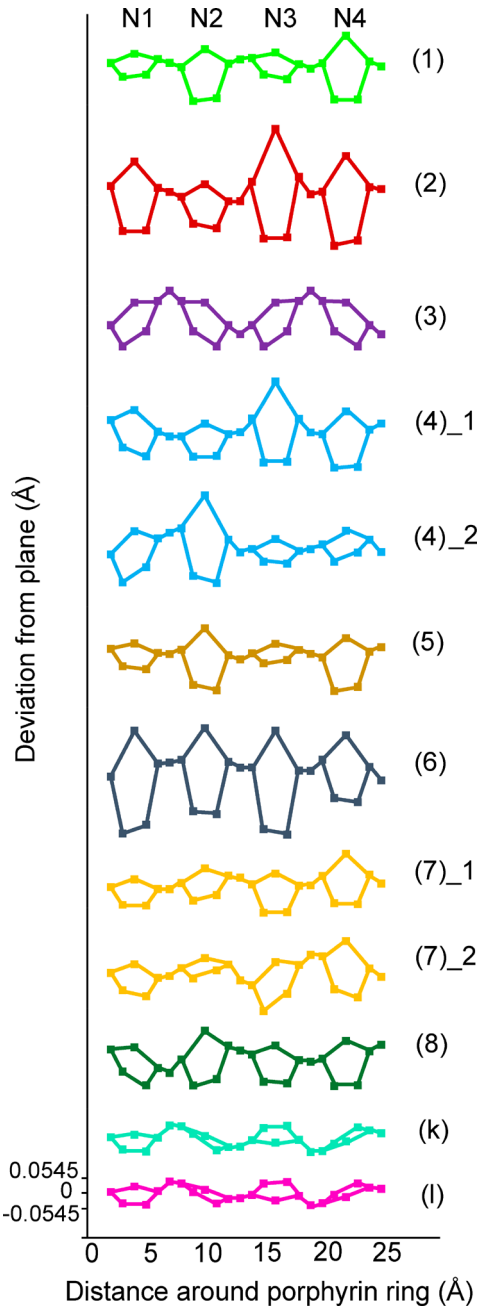

Figure 11. Comparison of the out-of-plane displacements of the porphyrin core atoms from the mean porphyrin plane as visualized in a linear fashion, for (Co^{II}(OEP)·C_{60}·CS_2 (**1**); Zn^{II}(OEP)·C_{60}·CS_2 (**2**); $ClCo^{III}$(OEP)·C_{60}·CCl_4 (**3**); the two symmetrically unrelated porphyrins in $2Zn^{II}$(OEP)·C_{60}·0.75CCl_4 (**4**)_**1** and (**4**)_**2**; Co^{II}(OEP)·C_{60}·$C_4H_8O_2$ (**5**); ($C_4H_8O_2$)Zn^{II}(OEP)·C_{60}·$C_4H_8O_2$ (**6**); the two symmetrically unrelated porphyrins in $2Co^{II}$(OEP)·C_{60}·C_4H_8O(**7**)_**1** and (**7**)_**2**; Co^{II}(OEP)·C_{60}·1.5C_6H_6 (**8**); (k) Co^{II}(OEP) (from data in Scheidt, W. R.; Turowska-Tyrk, I. *Inorg. Chem.* **1994**, *33*, 1314−1318). (l) Zn^{II}(OEP) (from data in Ozarowski, A.; Lee, H. M.; Balch, A. L. *J. Am. Chem. Soc.* **2003**, *125*, 12606−12614).

different structural types. As these data indicate, crystals with the 6 M^{II}(OEP) to 5 C_{60} ratio only form when dichloromethane or 1,2-dichloroethane is the solvent. Three other classes of new cocrystals have been prepared: Class 1 with ordered crystals with a 1:1 porphyrin/fullerene ratio including Co^{II}(OEP)·C_{60}·CS_2 (**1**), Zn^{II}(OEP)·C_{60}·CS_2 (**2**), Co^{II}(OEP)·C_{60}·$C_4H_8O_2$ (**5**), Co^{II}(OEP)·C_{60}·1.5C_6H_6 (**8**); Class 2 with ordered crystals with a 2:1 porphyrin/fullerene ratio including $2Zn^{II}$(OEP)·C_{60}·0.75CCl_4 (**4**) and $2Co^{II}$(OEP)·C_{60}·C_4H_8O (**7**); and Class 3 with a five-coordinate metal and a disordered fullerene cage including $ClCo^{III}$(OEP)·C_{60}·CCl_4 (**3**) and ($C_4H_8O_2$)Zn^{II}(OEP)·C_{60}·$C_4H_8O_2$ (**6**). Class 1 involves cocrystals forming in three different space groups, $P\bar{1}$, $I2/a$, and $P2_1/c$. Nevertheless, cocrystals in this class possess common structural features: the formation of extended columns as illustrated for Co^{II}(OEP)·C_{60}·CS_2 (**1**) in Figure 2 (and in Figures SI-1 to SI-3) and the formation of zigzag arrays of fullerenes as shown in Figure 3. However, the inclusion of differing solvate molecules results in crystallization of Class 1 cocrystals in different space groups with different symmetry elements generating the common patterns of intermolecular interactions.

All of the cocrystals in Class 2, which include some previously identified members ($2Co^{II}$(OEP)·C_{60}·$CHCl_3$,[8] $2Zn^{II}$(OEP)·C_{60}·$CHCl_3$,[8] and $2Zn^{II}$(OEP)·C_{60}·$2C_6H_6$[43]), are isostructural and crystallize in the space group $P2_12_12_1$. These Class 2 cocrystals have the clam-shell arrangements shown in Figures 4B, 6, and 9. With different axial ligands involved, it is not surprising that the two members of Class 3 crystallize in different space groups, but both cocrystals show a zigzag pattern of fullerene cages as seen in the packing diagrams in Figures 5 and 8. Cocrystallization of a five-coordinate porphyrin, LM(OEP), with C_{60} seems to be always accompanied by disorder in the fullerene. That is the case with the two structures, $ClCo^{III}$(OEP)·C_{60}·CCl_4 (**3**) and ($C_4H_8O_2$)Zn^{II}(OEP)·C_{60}·$C_4H_8O_2$ (**6**), reported here. Fullerene disorder is also found in other axially ligated porphyrins such as (CO)Ru^{II}(OEP)·C_{60}·$2C_6H_5CH_3$,[37] $ClFe^{III}$(OEP)·C_{60}·$CHCl_3$,[8] $ClIn^{III}$(OEP)·C_{60}·C_6H_6,[44] and Zn^{II}(OEP)-4,4′-bipyridine-Zn^{II}(OEP)·$2C_{60}$·$2CHCl_3$.[45] Consequently, five-coordinate LM(OEP) complexes would be poor choices to use if one wanted to produce cocrystals with ordered fullerenes.

CONCLUSIONS

Our results indicate that the choice of solvents utilized to grow cocrystals of M^{II}(OEP) with M = Co or Zn with C_{60} directs the composition and structure of the cocrystal that forms. The information in Table 3 also demonstrates the importance of the solvent and solvate molecules in determining the type of cocrystal that forms. Solvent, not the solution stoichiometry, determines the composition of the cocrystal that forms. In particular, our efforts to prepare crystals of Class 2 with a clamshell structure by altering the ratio of porphyrin to fullerene in the growth solution have not been successful. Although all of the cocrystals reported here have been obtained from a mixture of two solvents, it is remarkable that only one type of solvate molecule is found in each cocrystal. Despite the fact that the benzene-containing cocrystals Co^{II}(OEP)·C_{60}·1.5C_6H_6 (**8**) and Zn^{II}(OEP)·C_{60}·$2C_6H_6$[42] could have formed in the cases where carbon disulfide, carbon tetrachloride, dioxane, tetrahydrofuran, dichloromethane, 1,2-dichloroethane, or chloroform were used to dissolve the porphyrin, benzene was not incorporated into any of the cocrystals that formed. In cases where cocrystallization of a fullerene or endohedral fullerene with M^{II}(OEP) leads to a disordered structure as sometimes occurs, redissolving the sample in a different solvent mixture followed by slow evaporation may produce an entirely different cocrystal, which may not suffer from disorder. Additionally, it may be beneficial in such a case

https://dx.doi.org/10.1021/acs.cgd.0c00793
Cryst. Growth Des. 2020, 20, 5596−5609

Table 1. Distances Between Porphyrins

compound	metal−metal distance (Å)	interplanar distance (Å)	lateral shift (Å)	shortest out-of-plane metal−nitrogen distance (Å)	out-of-plane shift of metal (Å)
$Co^{II}(OEP)\cdot C_{60}\cdot CS_2$ (**1**)	3.4066(5)	3.165	1.569	2.883(2)	0.147
$Zn^{II}(OEP)\cdot C_{60}\cdot CS_2$ (**2**)	3.1118(7)	3.271	1.890	2.531(2)	0.422
$2Zn^{II}(OEP)\cdot C_{60}\cdot 0.75CCl_4$ (**4**)	3.1794 (8)	3.170	1.792	2.609 (3)	0.270, 0.330
$Co^{II}(OEP)\cdot C_{60}\cdot C_4H_8O_2$ (**5**)	3.4772(7)	3.182	1.392	2.9299(14)	0.130
$2Co^{II}(OEP)\cdot C_{60}\cdot C_4H_8O$ (**7**)	3.4367(8)	3.187	1.715	2.954(2)	0.103, 0.120
$Co^{II}(OEP)\cdot C_{60}\cdot 1.5C_6H_6$ (**8**)	3.4234(7)	3.199	1.705	2.963(2)	0.113
$Co^{II}(OEP)$[a]	4.742	3.333	3.373	3.648	0.000
$Zn^{II}(OEP)$[b]	4.692	3.339	3.014	3.596	0.000

[a]Data from Scheidt, W. R.; Turowska-Tyrk, I. *Inorg. Chem.* **1994**, 33, 1314−1318. [b]Data from Ozarowski, A.; Lee, H. M.; Balch, A. L. *J. Am. Chem. Soc.* **2003**, 125, 12606−12614.

Table 2. Contact Distances between Metal Centers and Fullerene Carbon Atoms

compound	metal to carbon atoms in 6:6 ring junctions (Å)	metal 6:6 centroid distance (Å)
$Co^{II}(OEP)\cdot C_{60}\cdot CS_2$ (**1**)	2.811(5), 2.976(4)	2.815
$Zn^{II}(OEP)\cdot C_{60}\cdot CS_2$ (**2**)	3.049(3), 3.241(3)	3.070
$2Zn^{II}(OEP)\cdot C_{60}\cdot 0.75CCl_4$ (**4**)	3.002(5), 3.230(5)	3.044
	2.917(4), 3.139(4)	2.950
$Co^{II}(OEP)\cdot C_{60}\cdot C_4H_8O_2$ (**5**)	2.7044(19), 3.081(2)	2.816
$(C_4H_8O_2)Zn^{II}(OEP)\cdot C_{60}\cdot C_4H_8O_2$ (**6**)	3.056(6), 3.248(6)	3.027
$2Co^{II}(OEP)\cdot C_{60}\cdot C_4H_8O$ (**7**)	2.657(3), 2.774(3)	2.625
	2.725(3), 3.139(3)	2.855
$Co^{II}(OEP)\cdot C_{60}\cdot 1.5C_6H_6$ (**8**)	2.671(3), 2.785(3)	2.640

Table 3. Porphyrin-Fullerene Stoichiometries and Crystallographic Space Groups for Cocrystals Formed with C_{60} and $Co^{II}(OEP)$ or $Zn^{II}(OEP)$

	Co(OEP)	Zn(OEP)
Carbon disulfide	1:1 $P\bar{1}$ **(1)**	1:1 $I2/a$ **(2)**
Carbon Tetrachloride	1:1 $Cmcm$ **(3)**	2:1 $P2_12_12_1$ **(4)**
Dioxane	1:1 $P2_1/c$ **(5)**	1:1 $P\bar{1}$ **(6)**
Tetrahydrofuran	2:1 $P2_12_12_1$ **(7)**	No cocrystal formed
Benzene	1:1 $P\bar{1}$ **(8)**	2:1 $P2_12_12_1$ QARQIJ
Dichloromethane	6:5 $P\bar{1}$ NOZFEQ	6:5 $P\bar{1}$ NOZFIU
1,2-Dichloroethane	6:5 $C2/m$ NOZFUG	6:5 $P\bar{1}$ NOZGAN
Chloroform	2:1 $P2_12_12_1$ CELTIW	2:1 $P2_12_12_1$ CELVAQ

Color scheme for structure types:- 2:1 clamshell, all-syn triclinic 1:1, all-syn monoclinic 1:1, 6:5 triclinic column with ordered unbound C_{60}, axially-coordinated $Co^{II}(OEP)$, axially coordinated $Zn^{II}(OEP)$, monoclinic 1:1 $Zn^{II}(OEP)$ with one anti ethyl arm. For previously reported cocrystals, the CCDC reference codes are given.

to utilize a different $M^{II}(OEP)$ that is likely to form a another type of cocrystal that may not suffer from disorder.

It is noteworthy that in the case of $Co^{II}(OEP)$, the 1:1 stoichiometry reoccurs, while in the case of $Zn^{II}(OEP)$, the 1:1 stoichiometry is less common than the 2:1 clamshell. It is, therefore, not a stretch to infer that barring unusual circumstances, $Zn^{II}(OEP)$ favors the 2:1 clamshell over other structure types with both benzene and chlorinated solvents (note: the **6:5Zn** columns formed from dichloromethane and dichloromethane still exhibit one clamshell per asymmetric unit). Since fullerenes in 2:1 clamshells experience the ordering influence of two symmetrically distinct porphyrins, they generally exhibit the smallest thermal ellipsoids. Because of the reoccurrence of this structure type with $Zn^{II}(OEP)$ and the unusually clean ordering of all fullerenes (even that unbound by a porphyrin) in the **6:5Zn** columnar structures, we have come to accept the confluence of $Zn^{II}(OEP)$ and chlorinated solvents as the most favorable combination when attempting to obtain well-ordered C_{60}, and this situation may pertain for other fullerenes.

Although solvate molecules are frequently encountered in crystals grown from solution, their presence is frequently regarded as a nuisance. Volatile solvate molecules often evaporate from the crystal, thereby causing a loss of crystallographic order. Modeling the disorder in solvate molecules often proves tedious. The role of solvate molecules in determining crystal stability and structure is difficult to comprehend unless well-recognized interactions such as hydrogen bonding, $\pi-\pi$, C−H−π interactions are present. Nevertheless, the presence of various solvate molecules can have significant influences on crystal composition, crystal structure, and molecular organization as shown here. Addi-

https://dx.doi.org/10.1021/acs.cgd.0c00793
Cryst. Growth Des. 2020, 20, 5596−5609

Table 4. Crystal Data for Cocrystals

	$Co^{II}(OEP)\cdot C_{60}\cdot CS_2$ (**1**)	$Zn^{II}(OEP)\cdot C_{60}\cdot CS_2$ (**2**)	$ClCo^{III}(OEP)\cdot C_{60}\cdot CCl_4$ (**3**)	$2Zn^{II}(OEP)\cdot C_{60}\cdot 0.75CCl_4$ (**4**)	$Co^{II}(OEP)\cdot C_{60}\cdot C_4H_8O_2$ (**5**)	$(C_4H_8O_2)Zn^{II}(OEP)\cdot C_{60}\cdot C_4H_8O_2$ (**6**)	$2Co^{II}(OEP)\cdot C_{60}\cdot C_4H_8O$ (**7**)	$Co^{II}(OEP)\cdot C_{60}\cdot 1.5C_6H_6$ (**8**)
chemical formula	$C_{97}H_{44}CoN_4S_2$	$C_{97}H_{44}N_4S_2Zn$	$C_{97}H_{44}Cl_5CoN_4$	$C_{132.75}H_{88}Cl_3N_8Zn_2$	$C_{100}H_{52}CoN_4O_2$	$C_{104}H_{60}N_4O_4Zn$	$C_{136}H_{96}Co_2N_8O$	$C_{105}H_{53}CoN_4$
formula weight	1388.41	1394.85	1501.54	2032.20	1400.38	1494.94	1976.06	1429.44
crystal system	triclinic	monoclinic	orthorhombic	orthorhombic	monoclinic	triclinic	orthorhombic	triclinic
space group	$P\bar{1}$	$I2/a$	$Cmcm$	$P2_12_12_1$	$P2_1/c$	$P\bar{1}$	$P2_12_12_1$	$P\bar{1}$
T (K)	90	100	100	90	100	100	100	100
a (Å)	14.1241(14)	23.976(3)	19.1369(8)	15.0603(6)	17.268(3)	13.8736(17)	14.7823(6)	14.6075(10)
b (Å)	14.4501(15)	14.6918(16)	20.8220(8)	20.8659(8)	14.926(2)	13.9361(18)	21.1096(9)	15.2328(11)
c (Å)	17.1030(17)	34.781(5)	15.7027(6)	29.4669(12)	24.525(4)	19.742(2)	29.1204(12)	16.5526(12)
α (deg)	75.831(2)	90	90	90	90	79.638(3)	90	74.4863(15)
β (deg)	74.429(2)	106.186(3)	90	90	107.847(3)	77.210(3)	90	72.9224(15)
γ (deg)	62.565(2)	90	90	90	90	62.751(3)	90	66.1709(15)
V (Å^3)	2954.3(5)	11766(2)	6257.0(4)	9259.9(6)	6016.9(16)	3295.7(7)	9087.0(7)	3173.7(4)
Z	2	8	4	4	4	2	4	2
μ (mm^{-1})	0.426	0.554	0.551	0.669	0.355	0.443	3.380	0.336
reflections collected	39158	101495	26171	196100	132691	97836	87540	77962
data/parameters/ restraints	15953/952/0	11867/963/14	5080/494/558	28445/1341/0	13269/972/0	24537/1604/1080	17881/1341/0	22969/1000/0
R_1 [data with $I > 2\sigma(I)$]	0.0717 [31890]	0.0481 [8469]	0.0479 [4624]	0.0472 [25078]	0.0399 [10661]	0.0457 [21668]	0.0343 [16856]	0.0497 [18568]
wR_2 (all data)	0.1809	0.1056	0.1288	0.1363	0.1043	0.1162	0.0788	0.1081

[a] $R_1 = \frac{\Sigma ||Fo| - |Fc||}{\Sigma |Fo|}$; $wR_2 = \left\{ \frac{\Sigma[w(Fo^2 - Fc^2)^2]}{\Sigma[w(Fo^2)^2]} \right\}^{1/2}$.

https://dx.doi.org/10.1021/acs.cgd.0c00793
Cryst. Growth Des. 2020, 20, 5596−5609

tionally, the presence of different solvate molecules has been shown to influence the structure and physical properties of other types of crystals such as the gold−gold interactions and luminescence of dimeric gold(I) complexes.[46−48] Solvate molecules also influence the magnetic properties of transition metal complexes.[49,50]

EXPERIMENTAL SECTION

Materials and General Consideration. H_2(OEP) was purchased from Frontier Scientific. Metalation of H_2(OEP) was accomplished by an established route.[51] C_{60} was purchased from SES Research with 99.5% purity. Solvents were obtained commercially and used as received.

Crystal Growth. In a clean scintillation vial, a 0.56 mmol solution of C_{60} in benzene was prepared by sonication for approximately 30 min. In a separate scintillation vial, an equal volume of a 0.56 mmol solution of M^{II}(OEP) in carbon disulfide, carbon tetrachloride, dioxane, or tetrahydrofuran was prepared. Cocrystallization was conducted in 5 mm diameter glass tubes. A 1.0 mL portion of the M^{II}(OEP) solution was carefully pipetted into the tube through a filter pipet. Subsequently, a 1.0 mL of the C_{60} solution in benzene was carefully layered over the M^{II}(OEP) solution after filtration through a fresh filter pipet. For each M^{II}(OEP) and solvent combination, the order of layering was reversed to ensure that this did not affect composition. The crystal tubes were capped with a rubber septum and left undisturbed in a dark cabinet until suitable crystal growth occurred. In each case, only one crystalline phase formed in the tube.

Crystal Structure Determinations. Crystallographic data are reported in Table 4. Crystals of compounds (**1**), (**2**), (**3**), (**5**), (**6**), (**7**), and (**8**) were mounted in the 90 K nitrogen cold stream provided by a CRYO Industries low-temperature apparatus on a Bruker Kappa DUO instrument equipped with a molybdenum microsource (λ = 0.71073 Å), except for (**7**) which collected using a copper microsource (λ = 1.54178 Å). Data for compound (**4**) were collected with use of a Bruker ApexII diffractometer equipped with a sealed molybdenum tube and a CRYO Industries low-temperature apparatus. All data sets were reduced with the use of Bruker SAINT, and a multiscan absorption correction was applied with the use of SADABS for compounds (**2**), (**3**), (**4**), (**5**), and (**7**), while TWINABS was used for absorption correction for compounds (**1**), (**6**), and (**8**). Structure solutions and refinements were conducted with SHELXT 2015[52] and SHELXL 2018.[53]

ASSOCIATED CONTENT

Supporting Information

The Supporting Information is available free of charge at https://pubs.acs.org/doi/10.1021/acs.cgd.0c00793.

Additional figures and numbering schemes for the porphyrin crystal structures (PDF)

Accession Codes

CCDC 1991772−1991778 and 2008493 contain the supplementary crystallographic data for this paper. These data can be obtained free of charge via www.ccdc.cam.ac.uk/data_request/cif, or by emailing data_request@ccdc.cam.ac.uk, or by contacting The Cambridge Crystallographic Data Centre, 12 Union Road, Cambridge CB2 1EZ, UK; fax: +44 1223 336033.

AUTHOR INFORMATION

Corresponding Authors

Marilyn M. Olmstead − *Department of Chemistry, University of California, Davis 95616, United States;* orcid.org/0000-0002-6160-1622; Phone: (530) 752-6668; Email: mmolmstead@ucdavis.edu; Fax: (530) 752-8995

Alan L. Balch − *Department of Chemistry, University of California, Davis 95616, United States;* orcid.org/0000-0002-8813-6281; Phone: (530) 752-0941; Email: albalch@ucdavis.edu; Fax: (530) 752-8995

Authors

Mrittika Roy − *Department of Chemistry, University of California, Davis 95616, United States*

Isaac D. Diaz Morillo − *Department of Chemistry, University of California, Davis 95616, United States*

Xian B. Carroll − *Department of Chemistry, University of California, Davis 95616, United States;* orcid.org/0000-0003-1950-6960

Complete contact information is available at: https://pubs.acs.org/10.1021/acs.cgd.0c00793

Notes

The authors declare no competing financial interest.

ACKNOWLEDGMENTS

We thank the National Science Foundation for financial support (Grant CHE-1807637 to A.L.B. and M.M.O.).

REFERENCES

(1) Kroto, H. W.; Heath, J. R.; O'Brien, S. C.; Curl, R. F.; Smalley, R. E. C_{60} − Buckminsterfullerene. *Nature* **1985**, *318*, 162−163.

(2) Krätschmer, W.; Lamb, L. D.; Fostiropoulos, K.; Huffman, D. R. Solid C_{60}: A New Form of Carbon. *Nature* **1990**, *347*, 354−358.

(3) Beer, F.; Gügel, A.; Martin, K.; Räder, J.; Müllen, K. High−yield reactive extraction of giant fullerenes from soot. *J. Mater. Chem.* **1997**, *7*, 1327−1330.

(4) Weis, P.; Hennrich, F.; Fischer, R.; Schneider, E. K.; Neumaier, M.; Kappes, M. M. Probing the structure of giant fullerenes by high resolution trapped ion mobility spectrometry. *Phys. Chem. Chem. Phys.* **2019**, *21*, 18877−18892.

(5) Liu, S.; Lu, Y.-J.; Kappes, M. M.; Ibers, J. A. *Science* **1991**, *254*, 408−410.

(6) Bürgi, H.-B.; Blanc, E.; Schwarzenbach, D.; Liu, S.; Lu, Y.-J.; Kappes, M. M.; Ibers, J. A. The Structure of C_{60} - Orientational Disorder in the Low-Temperature Modification of C_{60}. *Angew. Chem., Int. Ed. Engl.* **1992**, *31*, 640−643.

(7) Chancellor, C. J.; Bowles, F. L.; Franco, J. U.; Pham, D. M.; Rivera, M.; Sarina, E. A.; Ghiassi, K. B.; Balch, A. L.; Olmstead, M. M. Single-Crystal X-ray Diffraction Studies of Solvated Crystals of C_{60} Reveal the Intermolecular Interactions between the Component Molecules. *J. Phys. Chem. A* **2018**, *122*, 9626−9636.

(8) Olmstead, M. M.; Costa, D. A.; Maitra, K.; Noll, B. C.; Phillips, S. L.; Van Calcar, P. M.; Balch, A. L. Interaction of Curved and Flat Molecular Surfaces. The Structures of Crystalline Compounds Composed of Fullerene (C_{60}, $C_{60}O$, C_{70}, and $C_{120}O$) and Metal Octaethylporphyrin Units. *J. Am. Chem. Soc.* **1999**, *121*, 7090−7097.

(9) Stevenson, S.; Rice, G.; Glass, T.; Harich, K.; Cromer, F.; Jordan, M. R.; Craft, J.; Hadju, E.; Bible, R.; Olmstead, M. M.; Maitra, K.; Fisher, A. J.; Balch, A. L.; Dorn, H. C. Small-Bandgap Endohedral Metallofullerenes in High Yield and Purity. *Nature* **1999**, *401*, 55−57.

(10) Boyd, P. D. W.; Hodgson, M. C.; Rickard, C. E. F.; Oliver, A. G.; Chaker, L.; Brothers, P. J.; Bolskar, R. D.; Tham, F. S.; Reed, C. A. Selective Supramolecular Porphyrin/Fullerene Interactions. *J. Am. Chem. Soc.* **1999**, *121*, 10487−10495.

(11) Sun, D.; Tham, F. S.; Reed, C. A.; Chaker, L.; Boyd, P. D. W. Supramolecular Fullerene-Porphyrin Chemistry. Fullerene Complexation by Metalated "Jaws Porphyrin" Hosts. *J. Am. Chem. Soc.* **2002**, *124*, 6604−6612.

(12) Sun, D.; Tham, F. S.; Reed, C. A.; Boyd, P. D. W. Extending Supramolecular Fullerene-Porphyrin Chemistry to Pillared Metal-Organic Frameworks. *Proc. Natl. Acad. Sci. U. S. A.* **2002**, *99*, 5088−5092.

(13) Zheng, J.-Y.; Tashiro, K.; Hirabayashi, Y.; Kinbara, K.; Saigo, K.; Aida, T.; Sakamoto, S.; Yamaguchi, K. Cyclic Dimers of

Metalloporphyrins as Tunable Hosts for Fullerenes: A Remarkable Effect of Rhodium (III). *Angew. Chem., Int. Ed.* **2001**, *40*, 1857−1861.
(14) Nobukuni, H.; Shimazaki, Y.; Uno, H.; Naruta, Y.; Ohkubo, K.; Kojima, T.; Fukuzumi, S.; Seki, S.; Sakai, H.; Hasobe, T.; Tani, F. Supramolecular Structures and Photoelectronic Properties of the Inclusion Complex of a Cyclic Free-Base Porphyrin Dimer and C_{60}. *Chem. - Eur. J.* **2010**, *16*, 11611−11623.
(15) Wu, Z.-Q.; Shao, X.-B.; Li, C.; Hou, J.-L.; Wang, K.; Jiang, X.-K.; Li, Z.-T. J. Hydrogen-Bonding-Driven Preorganized Zinc Porphyrin Receptors for Efficient Complexation of C_{60}, C_{70}, and C_{60} Derivatives. *J. Am. Chem. Soc.* **2005**, *127*, 17460−17468.
(16) Yang, J.; Beavers, C. M.; Wang, Z.; Jiang, A.; Liu, Z.; Jin, H.; Mercado, B. Q.; Olmstead, M. M.; Balch, A. L. Isolation of a Small Carbon Nanotube: The Surprising Appearance of $D_{5h}(1)$-C_{90}. *Angew. Chem., Int. Ed.* **2010**, *49*, 886−890.
(17) Yang, H.; Mercado, B. Q.; Jin, H.; Wang, Z.; Jiang, A.; Liu, Z.; Beavers, C. M.; Olmstead, M. M.; Balch, A. L. Fullerenes without Symmetry: Crystallographic Characterization of $C_1(30)$-C_{90} and $C_1(32)$-C_{90}. *Chem. Commun.* **2011**, *47*, 2068−2070.
(18) Yang, H.; Jin, H.; Che, Y.; Hong, B.; Liu, Z.; Gharamaleki, J. A.; Olmstead, M. M.; Balch, A. L. Isolation of Four Isomers of C_{96} and Crystallographic Characterization of Nanotublular $D_{3d}(3)$-C_{96} and the Somewhat Flat-Sided Sphere $C_2(181)$-C_{96}. *Chem. - Eur. J.* **2012**, *18*, 2792−2796.
(19) Stevenson, S.; Mackey, M. A.; Stuart, M. A.; Phillips, J. P.; Easterling, M. L.; Chancellor, C. J.; Olmstead, M. M.; Balch, A. L. A Distorted Tetrahedral Metal Oxide Cluster inside an Icosahedral Carbon Cage, Synthesis, Isolation, and Structural Characterization of $Sc_4((_3\text{-}O)_2@I_h\text{-}C_{80}$. *J. Am. Chem. Soc.* **2008**, *130*, 11844−11845.
(20) Mercado, B. Q.; Olmstead, M. M.; Beavers, C. M.; Easterling, M. L.; Stevenson, S.; Mackey, M. A.; Coumbe, C. E.; Phillips, J. D.; Phillips, J. P.; Poblet, J. M.; Balch, A. L. A Seven Atom Cluster in a Carbon Cage, the Crystallographically Determined Structure of $Sc_4((_3\text{-}O)_3@I_h\text{-}C_{80}$. *Chem. Commun.* **2010**, *46*, 279−281.
(21) Mercado, B. Q.; Jiang, A.; Yang, H.; Wang, Z.; Jin, H.; Liu, Z.; Olmstead, M. M.; Balch, A. L. Isolation and Structural Characterization of the Molecular Nanocapsule, $Sm_2@D_{3d}(822)$-C_{104}. *Angew. Chem., Int. Ed.* **2009**, *48*, 9114−9116.
(22) Pan, C.; Bao, L.; Yu, X.; Fang, H.; Xie, Y.; Akasaka, T.; Lu, X. Facile Access to Y_2C_{2n} ($2n$ = 92−130) and Crystallographic Characterization of $Y_2C_2@C_1(1660)$-C_{108}: A Giant Nanocapsule with a Linear Carbide Cluster. *ACS Nano* **2018**, *12*, 2065−2069.
(23) Olmstead, M. M.; Lee, H. M.; Duchamp, J. C.; Stevenson, S.; Marciu, D.; Dorn, H. C.; Balch, A. L. $Sc_3N@C_{68}$: Folded Pentalene Coordination in an Endohedral Fullerene that Does Not Obey the Isolated Pentagon Rule. *Angew. Chem., Int. Ed.* **2003**, *42*, 900−903.
(24) Mercado, B. Q.; Beavers, C. M.; Olmstead, M. M.; Chaur, M. N.; Walker, K.; Holloway, B. C.; Echegoyen, L.; Balch, A. L. Is the Isolated Pentagon Rule Merely a Suggestion for Endohedral Fullerenes? The structure of a Second Egg-Shaped Endohedral Fullerene − $Gd_3N@C_s(39663)$−C_{82}. *J. Am. Chem. Soc.* **2008**, *130*, 7854−7855.
(25) Yamada, M.; Kurihara, H.; Suzuki, M.; Guo, J. D.; Waelchli, M.; Olmstead, M. M.; Balch, A. L.; Nagase, S.; Maeda, Y.; Hasegawa, T.; Lu, X.; Akasaka, T. $Sc_2@C_{66}$ Revisited: An Endohedral Fullerene with Scandium Ions Nestled within Two Unsaturated Linear Triquinanes. *J. Am. Chem. Soc.* **2014**, *136*, 7611−7614.
(26) Zhang, Y.; Ghiassi, K. B.; Deng, Q.; Samoylova, N. A.; Olmstead, M. M.; Balch, A. L.; Popov, A. A. Synthesis and Structure of $LaSc_2N@C_s(hept)$-C_{80} with One Heptagon and Thirteen Pentagons. *Angew. Chem., Int. Ed.* **2015**, *54*, 495−499.
(27) Chen, C.-H.; Abella, L.; Cerón, M. R.; Guerrero-Ayala, M. A.; Rodríguez-Fortea, A.; Olmstead, M. M.; Powers, X. B.; Balch, A. L.; Poblet, J. M.; Echegoyen, L. Zigzag Sc_2C_2 Carbide Cluster inside a [88]Fullerene Cage with One Heptagon, $Sc_2C_2@C_s(hept)$-C_{88}: A Kinetically Trapped Fullerene Formed by C_2 Insertion? *J. Am. Chem. Soc.* **2016**, *138*, 13030−13037.
(28) Hu, S.; Shen, W.; Zhao, P.; Xu, T.; Slanina, Z.; Ehara, M.; Zhao, X.; Xie, Y.; Akasaka, T.; Lu, X. Crystallographic characterization of $Er_2C_2@C_2(43)$-C_{90}, $Er_2C_2@C_2(40)$-C_{90}, $Er_2C_2@C_2(44)$-C_{90}, and $Er_2C_2@C_1(21)$-C_{90}: the role of cage-shape on cluster configuration. *Nanoscale* **2019**, *11*, 17319−17326.
(29) Yang, W.; Velkos, G.; Liu, F.; Sudarkova, S. M.; Wang, Y.; Zhuang, J.; Zhang, H.; Li, X.; Zhang, X.; Büchner, B.; Avdoshenko, S. M.; Popov, A. A.; Chen, N. Single Molecule Magnetism with Strong Magnetic Anisotropy and Enhanced Dy···Dy Coupling in Three Isomers of Dy-Oxide Clusterfullerene $Dy_2O@C_{82}$. *Adv. Sci.* **2019**, *6*, 1901352.
(30) Zhuang, J.; Abella, L.; Sergentu, D.-C.; Yao, Y.-R.; Jin, M.; Yang, W.; Zhang, X.; Li, X.; Zhang, D.; Zhao, Y.; Li, X.; Wang, S.; Echegoyen, L.; Autschbach, J.; Chen, N. Diuranium(IV) Carbide Cluster U_2C_2 Stabilized Inside Fullerene Cages. *J. Am. Chem. Soc.* **2019**, *141*, 20249−20260.
(31) Hao, Y.; Feng, L.; Xu, W.; Gu, Z.; Hu, Z.; Shi, Z.; Slanina, Z.; Uhlík, F. $Sm@C_{2v}$ (19138)-C_{76}: A Non-IPR Cage Stabilized by a Divalent Metal Ion. *Inorg. Chem.* **2015**, *54*, 4243−4248.
(32) Futagoishi, T.; Murata, M.; Wakamiya, A.; Sasamori, T.; Murata, Y. Expansion of Orifices of Open C_{60} Derivatives and Formation of an Open $C_{59}S$ Derivative by Reaction with Sulfur. *Org. Lett.* **2013**, *15*, 2750−2753.
(33) Zhang, R.; Murata, M.; Wakamiya, A.; Murata, Y. Synthesis and Structure of an Open-cage $C_{69}O$ Derivative. *Chem. Lett.* **2017**, *46*, 543−546.
(34) Roy, M.; Olmstead, M. M.; Balch, A. L. Metal Ion Effects on Fullerene/Porphyrin Cocrystallization. *Cryst. Growth Des.* **2019**, *19*, 6743−6751.
(35) Balch, A. L.; Lee, J. W.; Noll, B. C.; Olmstead, M. M. Disorder in a Crystalline Form of Buckministerfullerene: C60·4C6H6. *J. Chem. Soc., Chem. Commun.* **1993**, 56−58.
(36) Bürgi, H. B.; Restori, R.; Schwarzenbach, D.; Balch, A. L.; Lee, J. W.; Noll, B. C.; Olmstead, M. M. Nanocrystalline Domains of a Monoclinic Modification of Benzene Stabilized in a Crystalline Matrix of C60. *Chem. Mater.* **1994**, *6*, 1325−1329.
(37) Cullen, D. L.; Meyer, E. F., Jr. The Crystal and Molecular Structure of 2,3,7,8,12,13,17,18-Octaethylporphinatomonopyridine-zinc(II).). *Acta Crystallogr., Sect. B: Struct. Crystallogr. Cryst. Chem.* **1976**, *32*, 2259−2269.
(38) Konarev, D. V.; Khasanov, S. S.; Saito, G.; Lyubovskaya, R. N. Design of Molecular and Ionic Complexes of Fullerene C_{60} with Metal(II) Octaethylporphyrins, MOEP (M = Zn, Co, Fe, and Mn) Containing Coordination M-N(ligand) and M-C(C_{60}^-) Bonds. *Cryst. Growth Des.* **2009**, *9*, 1170−1181.
(39) Shelnutt, J. A.; Song, X.-Z.; Ma, J.-G.; Jia, S.-G.; Jentzen, W.; Medforth, C. J. Nonplanar porphyrins and their significance in proteins. *Chem. Soc. Rev.* **1998**, *27*, 31−41.
(40) Scheidt, W. R.; Turowska-Tyrk, I. Crystal and Molecular Structure of (Octaethylporphinato)cobalt(II). Comparison of the Structures of Four-Coordinate M(TPP) and M(OEP) Derivatives (M = Fe-Cu). Use of Area Detector Data. *Inorg. Chem.* **1994**, *33*, 1314−1318.
(41) Ozarowski, A.; Lee, H. M.; Balch, A. L. Crystal Environments Probed by EPR Spectroscopy. Variations in the EPR Spectra of Co^{II}(octaethylporphyrin) Doped in Crystalline Diamagnetic Hosts and a Reassessment of the Electronic Structure of Four-Coordinate Cobalt(II). *J. Am. Chem. Soc.* **2003**, *125*, 12606−12614.
(42) Scheidt, W. R.; Lee, Y. J. Recent Advances in the Stereochemistry of Metallotetrapyrroles. *Struct. Bonding (Berlin)* **1987**, *64*, 1−70.
(43) Ishii, T.; Aizawa, N.; Yamashita, M.; Matsuzaka, H.; Kodama, T.; Kikuchi, K.; Ikemoto, I.; Iwasa, Y. First Syntheses of Cocrystallites Consisting of *Anti*-formed Metal Octaethylporphyrins with Fullerene C_{60}. *J. Chem. Soc., Dalton Trans.* **2000**, 4407−4412.
(44) Garcia, T. Y.; Olmstead, M. M.; Fettinger, J. C.; Balch, A. L. Crystallization of Chloroindium(III)octaethylporphyrin Into a Clam-shell Motif to Engulf Guest Molecules. *CrystEngComm* **2010**, *12*, 866−871.
(45) Konarev, D. V.; Khasanov, S. S.; Slovokhotov, Y. L.; Saito, G.; Lyubovskaya, R. N. Neutral and Ionic Complexes of C_{60} with

https://dx.doi.org/10.1021/acs.cgd.0c00793
Cryst. Growth Des. 2020, 20, 5596−5609

(ZnOEP)$_2$·BPy Coordination Dimers. *CrystEngComm* **2008**, *10*, 48−53.
(46) Lim, S. H.; Olmstead, M. M.; Balch, A. L. Molecular Accordion: Vapoluminescence and Molecular Flexibility in the Orange and Green Luminscent Crystals of the Dimer, Au_2(>-bis-(diphenylphosphino)ethane)$_2Br_2$. *J. Am. Chem. Soc.* **2011**, *133*, 10229−10238.
(47) Lim, S. H.; Olmstead, M. M.; Balch, A. L. Inorganic topochemistry. Vapor-induced solid state transformations of luminescent, three-coordinate gold(I) complexes. *Chem. Sci.* **2013**, *4*, 311−318.
(48) England, K. R.; Lim, S. H.; Luong, L. M. C.; Olmstead, M. M.; Balch, A. L. Vapoluminescent Behavior and the Single-Crystal-to-Single-Crystal Transformations of Chloroform Solvates of [Au_2((−1,2-bis(diphenylarsino)ethane)$_2$](AsF_6)$_2$. *Chem. - Eur. J.* **2019**, *25*, 874−878.
(49) Djemel, A.; Stefanczyk, O.; Marchivie, M.; Trzop, E.; Collet, E.; Desplanches, C.; Delimi, R.; Chastanet, G. Solvatomorphism-Induced 45 K Hysteresis Width in a Spin-Crossover Mononuclear Compound. *Chem. - Eur. J.* **2018**, *24*, 14760−14767.
(50) Sun, X.-P.; Wei, R.-J.; Yao, Z.-S.; Tao, J. Solvent Effects on the Structural Packing and Spin-Crossover Properties of a Mononuclear Iron(II) Complex. *Cryst. Growth Des.* **2018**, *18*, 6853−6862.
(51) Asano, M.; Kaizu, Y.; Kobayashi, H. The lowest excited states of copper porphyrins. *J. Chem. Phys.* **1988**, *89*, 6567−6576.
(52) Sheldrick, G. M. SHELXT − Integrated space-group and crystal-structure determination. S. *Acta Crystallogr., Sect. A: Found. Adv.* **2015**, *71*, 3−8.
(53) Sheldrick, G. M. *SHELXL* 2018/3. Crystal structure refinement with SHELXL. *Acta Crystallogr., Sect. C: Struct. Chem.* **2015**, *71*, 3−8.

https://dx.doi.org/10.1021/acs.cgd.0c00793
Cryst. Growth Des. 2020, 20, 5596−5609